The Journal of Chemical Physics ARTICLE pubs.aip.org/aip/jcp

Salt induced slowdown of kinetics and dynamics during thermal gelation of egg-yolk

Cite as: J. Chem. Phys. 161, 055102 (2024); doi: 10.1063/5.0219004
Submitted: 14 May 2024 • Accepted: 22 July 2024 •
Published Online: 6 August 2024

Nimmi Das Anthuparambil,[1,a] Sonja Timmermann,[1] Michelle Dargasz,[1] Sebastian Retzbach,[2] Maximilian D. Senft,[2] Nafisa Begam,[2,3] Anastasia Ragulskaya,[2] Michael Paulus,[4] Fajun Zhang,[2] Fabian Westermeier,[5] Michael Sprung,[5] Frank Schreiber,[2] and Christian Gutt[1,b]

AFFILIATIONS

[1] Department Physik, Universität Siegen, 57072 Siegen, Germany
[2] Institut für Angewandte Physik, Universität Tübingen, 72076 Tübingen, Germany
[3] Department of Physics, Banaras Hindu University, Varanasi 221005, India
[4] Fakultät Physik/DELTA, Technische Universität Dortmund, 44221 Dortmund, Germany
[5] Deutsches Elektronen-Synchrotron DESY, 22607 Hamburg, Germany

[a] Author to whom correspondence should be addressed: nimmi.anthuparambil@uni-siegen.de
[b] Electronic mail: christian.gutt@uni-siegen.de

ABSTRACT

We investigated the effect of the NaCl concentration (0.3–2M) on the structure and dynamics of hen egg yolk at room temperature and during thermal gelation at temperatures in the range of 66–90 °C utilizing low-dose x-ray photon correlation spectroscopy in ultra-small angle x-ray scattering geometry. With an increase in the salt concentration, we observe progressive structural and dynamic changes at room temperature, indicating the disruption of yolk components such as yolk-granules and yolk-plasma proteins. Temperature- and salt-dependent structural and dynamic investigations suggest a delay in the gel formation and aggregation of yolk low-density lipoproteins with increasing ionic strength. However, the time–temperature superposition relationship observed in all samples suggests an identical mechanism underlying protein aggregation–gelation with a temperature-dependent reaction rate. The sol–gel transition time extracted from kinetic and dynamic information follows Arrhenius's behavior, and the activation energy (460 kJ/mol) is found to be independent of the salt concentration.

I. INTRODUCTION

Gelation is an important functional property of proteins with numerous applications in food,[1–3] pharmaceutics,[4,5] and biotechnology.[6,7] Gelation of proteins can be induced or altered by physical (heating,[8–10] freezing,[11,12] and high pressure[13,14]), chemical (salt,[15–21] pH,[14,22–24] and others[25]), and biochemical (enzyme[26]) methods. These methods affect gel formation by altering protein structure and intermolecular interactions between proteins and proteins with solvent molecules. This leads to changes in the final gel texture, gel strength, water-holding capacity, and other properties of the gel.[27–31] This implies that gel characteristics can be tailored to specific applications by changing the gelation pathway using additives.[32,33] An in-depth knowledge of how additives influence the gelation pathway to achieve the desired gel characteristics by altering protein–protein and protein–solvent interactions is required for a fundamental understanding of the gelation process as well as for various applications.

Full egg yolks and egg yolk fractions (yolk-plasma and yolk-granule) are popular and versatile ingredients used in the food industry,[34,35] biotechnology,[2,36] and other fields.[2] The high concentration and diversity of proteins and lipids in egg yolk serve as a material foundation for its functional features' gelation, coagulation, foaming, and emulsification.[2,16,37,38] NaCl is frequently added during the processing of egg-containing food products to enhance taste, inhibit microbial growth,[39] and stabilize the emulsion.[40,41] The addition of NaCl to egg yolk affects its emulsification capacity and viscosity.[42,43] Furthermore, salted egg yolks are heated to

produce many food items, such as egg yolk based pastries. In general, the addition of salt to protein solutions is found to promote[15–19] or delay[20,21] heat-induced denaturation and gelation. For example, salt is added to protein aggregates to induce cold gelation.[44–46] In such cases, gelation is induced by reducing the electrostatic repulsion between the aggregates. However, in some cases, salt is found to stabilize the quaternary structure of proteins[47,48] and, thus, delay denaturation and further gelation. Furthermore, sodium chloride can change the characteristics of gels by strengthening or weakening interactions between protein molecules.[49] While there have been reports on the impact of salt,[17,29–31,50] pH,[27,44] and temperature[10,16] on rheological qualities and gel strength, little attention has been devoted to understand how an increase in ionic strength leads to changes in the structure and dynamics of protein, or protein–lipid systems.

In the past, rheology[16,29,44,51] and microscopy[29,44,51] were largely used to investigate the evolution of viscoelastic properties and microstructure during the gelation process in the presence of additives such as salt and acids. However, the evolution of the structure and dynamics of individual yolk components during heating at various ionic strengths is poorly understood. Moreover, the denaturation and aggregation of small proteins occur at nanometer to micrometer length scales, and hence, these processes need to be understood at the relevant length and time scales. In certain cases, it is often challenging to investigate such processes due to the complexity of multi-component protein samples and the requirement to concurrently observe a wide window of length and time scales. To tackle these problems, we utilize low-dose x-ray photon correlation spectroscopy (XPCS), which allows us to simultaneously follow structural and dynamical changes in the system in an *in situ* heating experiment. XPCS is widely used to study the relaxation dynamics of proteins,[52–58] polymers,[59–61] colloids,[62] glasses,[63] and many hard[64] and soft materials.[65] In particular, our previous investigation on the thermal gelation of egg yolk has contributed to the understanding of spatiotemporal scaling laws and time–temperature relationships underlying the process of thermal denaturation, aggregation, and gelation.

Here, we study the effect of the NaCl concentration on the thermal gelation of egg yolk utilizing XPCS experiments in ultra-small angle x-ray scattering geometry (USAXS). We observe a reduction in the rate of heat-induced protein denaturation, aggregation, and gelation with an increase in the salt concentration. However, the activation energy barrier of these processes is not significantly affected by the presence of salt. Our research provides information on changes in the spatiotemporal scaling laws underlying these non-equilibrium processes in the presence of salt ions. This work emphasizes the tunability of sol–gel transition time by changing ionic strength in a protein–lipid system, which is relevant for fundamental physics as well as for applications in food, pharmaceuticals, and bionanotechnology.

II. EXPERIMENTAL

A. Sample details

The egg yolk used in this study was extracted from a hen egg bought from a local supermarket. The extraction of the yolk was performed in the following manner: step 1: egg yolk was separated from egg white using a steel strainer and then washed in Milli-Q water to remove extra albumen from the yolk. Step 2: the cleaned yolk was transferred onto a filter paper to absorb extra water and albumen on the surface. Complete removal of water and albumen was achieved by rolling the yolk on the filter paper a few times. Step 3: the vitelline membrane was pierced using a plastic pipette tip, and the yolk was extracted and stored in a 15 ml falcon tube at 5 °C.

To separate the yolk plasma from the yolk granules, the egg yolk is centrifuged[37] at 7197 rcf for ≈48 h. After centrifugation, yolk-granules were sedimented in the solution, leaving a yellow-translucent liquid (egg yolk-plasma) on top [Fig. 3(b), inset]. The major constituent of egg yolk-plasma is low-density lipoproteins (LDLs) (85% of yolk-plasma), which are water-soluble entities with a density of 0.982 g cm^{-3}. The LDLs have a core–shell structure, as depicted in Fig. 1(a). The core is made of triglycerides and cholesterol esters in a liquid state, and the shell consists of a mono-film of phospholipids onto which apolipoproteins adhere. The average diameter of LDL is ≈30 nm. Egg yolk-granules have a light yellow color compared to plasma, as depicted in Fig. 3(b). The egg yolk-granules were diluted with Milli-Q water to a concentration of 910 mg/ml for the XPCS measurements. Egg yolk-granules are spherical complexes with a diameter of ≈ 0.3–2 μm. They are made up of LDLs, high-density lipoproteins (HDLs), and a protein called phosvitin.[72]

To investigate the effect of ionic strength on gelation kinetics and dynamics of egg yolk, NaCl powder (purchased from Carl Roth GmbH) at different concentrations (see Table I) was added to the yolk solution and kept for mixing using a magnetic stirrer for 12 h. The mixed samples were stored in a freezer at 5 °C for up to 2 days of experimental duration. In the present study, the experiments were performed 0–2 days after the addition of salt, and there could be some additional effects if the samples were stored for longer periods.[16] The samples were transferred into quartz-glass capillaries of diameter 1.5 mm. The capillaries were sealed with parafilm and placed in the Linkam heating stage for performing USAXS–XPCS, as depicted in Fig. 1. The yolk samples were heated to temperatures in the range of 66–77 °C. Yolkplasma samples were heated to 90 °C. The samples were heated from 22 °C to the desired set temperature with a constant ramp of 150 °C/min. The temperature calibration of the heating stage is provided in the supplementary material. The time taken to reach the set temperature of 22 °C is denoted by $t_{heating}$. Two time scales are used throughout the text: isothermal waiting time t_w and absolute waiting time t'_w, which are related via $t_w = t'_w - t_{heating}$. Here, $t'_w = 0$ denotes the onset of heating.

B. Coherent x-ray scattering experiments

The low-dose USAXS–XPCS[52] measurements were performed at beamline P10 of PETRA III, DESY, Hamburg, Germany. The schematic of the experiment is shown in Fig. 1(a). An x-ray beam of size 100 × 100 μm^2 and photon energy of 8.54 keV is incident on the sample-capillary placed inside the Linkam heating cell (Linkam Scientific Instruments Ltd., UK) in transmission geometry. The scattered x-rays are collected using an EIGER X4M area detector (pixel size = 75 × 75 μm^2) placed at a distance of 21.2 m downstream of the sample. This geometry provides access to a q-range of 0.005–0.22 nm^{-1}. A typical scattering pattern from the experiment

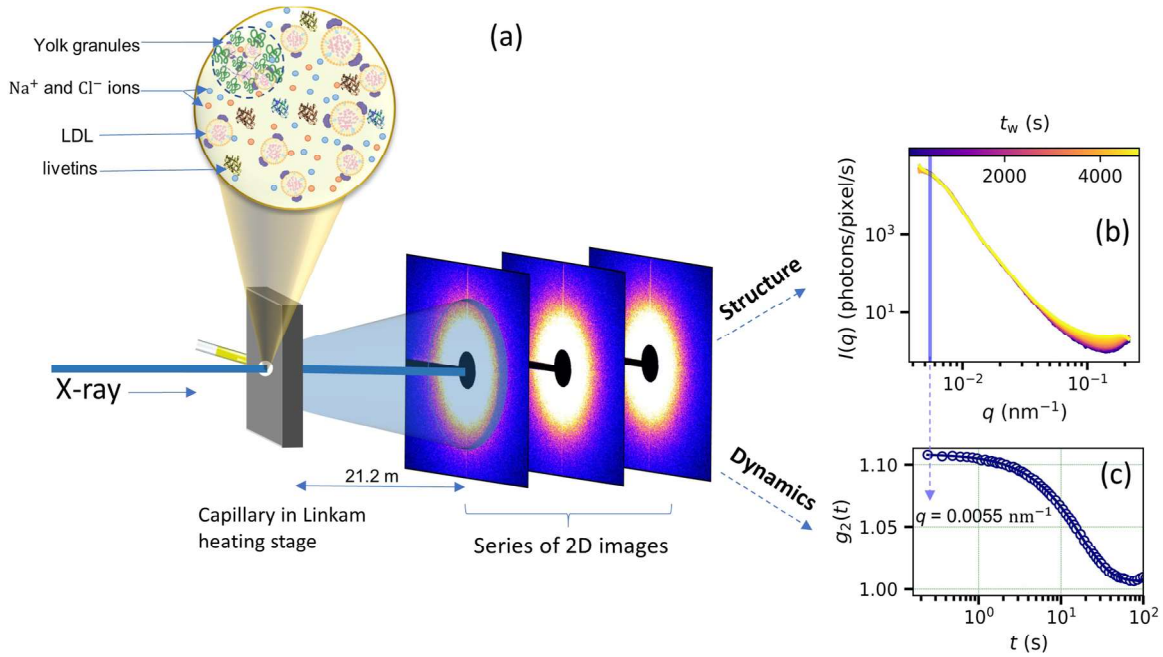

FIG. 1. (a) A coherent x-ray beam from a synchrotron source is scattered by the yolk sample contained in a quartz-glass capillary in transmission geometry. A 2D detector is used to collect a time series of speckle patterns at a distance of 21.2 m from the sample. Various components in a salted egg yolk are shown in the top schematic. Egg yolk contains ≈52% of water and ≈48% dry matter constituting LDLs, yolk-granules, and a variety of proteins (livetins).[37] The LDLs constitute ≈66% of total dry matter, and they have a core–shell structure (average diameter ≈ 30 nm).[2,37,66] The core of LDL is made of lipids (triglycerides, cholesterol esters, and free cholesterol), which are surrounded by a shell of phospholipids, cholesterol, and apolipoproteins.[2] The egg yolk-granules constitute ≈22% of total dry matter and are spherical complexes (diameter ≈ 0.3–2 μm[67–69]) made of LDLs, high-density lipoproteins (HDLs), and a protein called phosvitin.[70,71] Parts of this schematic were created with Biorender.com. (b) Time-resolved scattering intensity curves reveal the structural changes during an *in situ* heating experiment. The scattering intensities shown here are from pure yolk. (c) The intensity autocorrelation function at a specific q value provides information about the sample dynamics.

TABLE I. Sample details.

Sample	Amount of yolk[a] (g)	Amount of salt (mg)	Salt molarity (mM)
Yolk	2.04	0.0	0
y300	2.04	18.6	300
y500	2.04	31.0	500
y800	2.04	49.6	800
y1000	2.04	62.0	1000
y1500	2.04	93.0	1500
y2000	2.04	124.0	2000
y3000	2.04	186.0	3000

[a]Amount of yolk in the stock solution. The water content in the yolk is ≈52%.

is shown in Fig. 1(a). The azimuthally integrated scattering intensity $I(q)$ provides information about the structural changes in the sample [Fig. 1(b)].

According to recent research, radiation damage causes structural and dynamical changes in protein samples.[55,73–75] To prevent radiation damage from over-exposure, the capillaries were shifted laterally by 200 μm between two successive measurements across the x-ray beam. In addition, an optimal configuration of silicon absorbers was placed in front of the sample, and a total exposure time was selected to limit the total absorbed dosage. In particular, all measurements presented in this study were performed using dose rates of 0.024 kGy/s and 0.082 kGy/s, and the absorbed dose per scan was limited to 5 kGy (see the supplementary material for more details). The data extraction and analysis were performed using a Python-based analysis package—Xana,[76] and a MATLAB-based package—XPCSGUI, provided by the P10 beamline.

The time-resolved sample dynamics is extracted via two-time correlation functions (TTCs),[53,56,64,77–80]

$$C(q,t_1,t_2) = \frac{\langle I_{\text{pixel}}(q,t_1) I_{\text{pixel}}(q,t_2)\rangle}{\langle I_{\text{pixel}}(q,t_1)\rangle \langle I_{\text{pixel}}(q,t_2)\rangle}, \quad (1)$$

where I_{pixel} is the intensity at a given point, $\langle \ldots \rangle$ denotes the average over pixels in a q-range of $q \pm \delta q$, and t_1 and t_2 are the different experimental times. Here, the scattering wavevector q is given by $(4\pi/\lambda)\sin(\theta)$, where 2θ is the scattering angle and λ is the wavelength of the x-rays.

The absolute waiting time, t'_w, increases along the diagonal ($t_1 = t_2$) of a TTC (as displayed in Fig. 9), and $t'_w = 0$ indicates the onset of heating. The relative time $t = |t_1 - t_2|$ increases away from the diagonal in the off-diagonal direction. The time-resolved one-time autocorrelation function, $g_2(q,t,t'_w)$ at different t'_w are obtained from the TTCs via diagonal cuts[77,81] $[C(q,t,t'_w)]$ along t'_w, as shown

in Fig. 9(a). A typical g_2 function extracted from the scattering intensity fluctuations is shown in Fig. 1(c). The $g_2(q,t,t'_w)$ are modeled using the relation[82]

$$g_2(q,t,t'_w) = 1 + \beta|f(q,t)|^2 = 1 + \beta|\exp\left[-(t/\tau(q))^{\gamma}\right]|^2, \quad (2)$$

where $f(q,t)$, $\tau(q)$, β, and γ are the intermediate scattering function (ISF), relaxation time, speckle contrast, and Kohlrausch–Williams–Watts (KWW) exponent,[83] respectively.

Here, the exponent γ determines the shape of g_2 functions and provides information about the nature of the dynamics. An exponentially decaying correlation function ($\gamma = 1$) together with $\tau(q) \propto q^{-2}$ is the hallmark of Brownian motion, while compressed exponential g_2 functions ($\gamma > 1$) are typically found in arrested and/or out-of-equilibrium systems such as gels, foams, and glasses[84–86] but also in solid state systems with stress-driven dynamics.[87] Heterogeneous dynamics, for example, caused by polydispersity or differently evolving regions in the sample, often lead to stretched exponential decays ($\gamma < 1$).[84]

III. RESULTS AND DISCUSSION

A. Structural and dynamical changes in egg yolk with an increase in the NaCl concentration at T = 22 °C

Hen egg yolk is a highly heterogeneous, multi-component, crowded sample system with natural nano- and micrometer assemblies that are balanced by the subtle interplay of the interactions between proteins, phospholipids, cholesterol, and water. A typical scattering intensity $I(q)$ curve of egg yolk is depicted in Fig. 2(a). The key features are (i) $I(q) \propto q^{-4}$ at lower q values, indicating Porod-scattering from the spherical yolk-granules, and (ii) structure factor peak at $q = 0.22$ nm^{-1}, originated from the LDL particles[52] (see also Fig. S3 of the supplementary material). Upon the addition of NaCl, subtle changes occur in the $I(q)$ curves, indicating changes to the individual yolk components.

First, the Porod regime is shifted to the lower q region, and a new regime appears between the Porod and the peak at $q = 0.22$ nm^{-1}. To quantify these changes, we fit the $I(q)$ at low and high q values using $I(q) \propto q^{-p1}$ and $I(q) \propto q^{-p2}$, respectively.

In pure yolk, we observe a power law exponent of p1 = 4, indicative of Porod scattering from the sharp interface of the yolk granules in the non-salted environment. Note that the radius of yolk granules is $R \approx 1$ μm,[67–69] and thus, Porod scattering is expected for $q > \pi/R \approx 0.003$ nm^{-1}.[88] With the addition of salt, the exponent decreases to values of p1 = 3, which indicates a fractal or rough surface[89,90] of the yolk granules, indicative of the deterioration of the structure of the yolk granules. At larger q-values between 0.03 and 0.15 nm^{-1}, we observe a new power law regime appearing in the scattering intensity upon the addition of salt. The corresponding exponent p2 increases from values of 0.6–1.5 with increasing salt concentration. This may be connected to the breakdown of the micrometer-sized granules into smaller granular species, leading to enhanced scattering in this q-range upon the addition of salt [Fig. 2(a)].

These results are reproducible in the pure yolk-granule data shown in Fig. 3(b). It is noted that with the addition of NaCl, the color of the egg yolk changes from turbid yellow to partially transparent yellow. Yolk-granules cause egg yolk turbidity, and a decrease in turbidity does signify the breakdown of yolk-granules.[91,92] It is also reported that at high salt concentrations, the phosphocalcic bridges in yolk-granules are broken due to the replacement of Ca^{2+} ions by Na^{+} ions, and phosvitin and HDL are solubilized.[93]

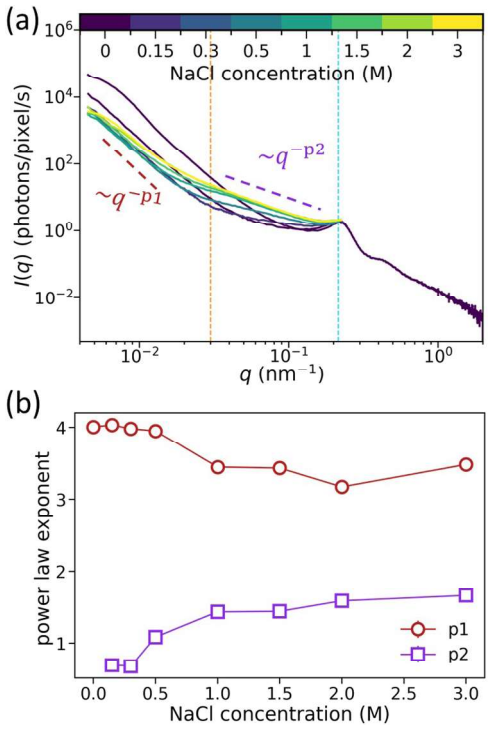

FIG. 2. (a) Scattering intensity of egg yolk at different NaCl concentrations at T = 22 °C. The concentrations are displayed on the color scale. At lower and higher q values, $I(q)$ follows $I(q) \propto q^{-p1}$ and $I(q) \propto q^{-p2}$, respectively, which are indicated using dashed lines. The orange and blue vertical lines indicate the q values of 0.03 and 0.22 nm^{-1}, respectively. (b) The power law exponents p1 and p2 as a function of the NaCl concentration.

Second, the addition of salt does not seem to change the overall spherical shape of LDL particles, as illustrated by constant scattering intensity values close to the structure factor peak of LDL at $q = 0.22$ nm^{-1} [Fig. 3(b)]. Earlier works[16] report rupture or aggregation of LDLs in the presence of NaCl. Note that most of these observations[16] were made after storing the yolk for longer durations, and in the present study, the experiments were performed 0–2 days after the addition of salt. Furthermore, there is an increase in $I(q)$ in the q-region 0.01–0.15 nm^{-1} of yolk-plasma [Fig. 3(b)]. Such $I(q)$ changes are observed during heat-induced denaturation of yolk-plasma proteins.[52] Hence, we anticipate that the addition of NaCl leads to structural modifications of yolk-plasma proteins.

Next, we discuss the changes in the collective dynamics of egg yolk with an increase in the salt concentration. Wave-vector dependent intermediate scattering functions of yolk without and with NaCl (2M) are compared in Figs. 4(a) and 4(b), respectively. There is a pronounced slow-down in the dynamics of yolk at lower q values

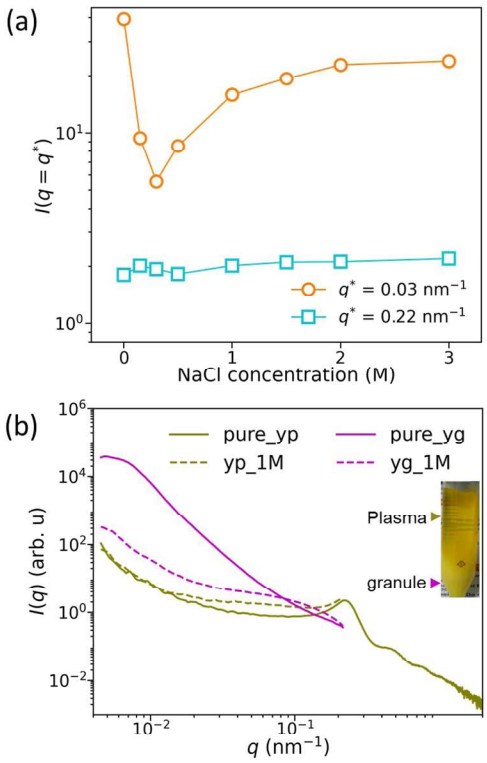

FIG. 3. (a) $I(q)$ at q = 0.03 nm^{-1} and q = 0.22 nm^{-1} as a function of the NaCl concentration at T = 22 °C. (b) $I(q)$ of yolk-plasma and yolk-granules without and with NaCl (concentration: 1M) at T = 22 °C. Meaning of the legend: yp: yolk-plasma and yg: yolk-granule. The inset image shows the yolk-plasma and yolk-granules separated after centrifugation of the egg yolk.

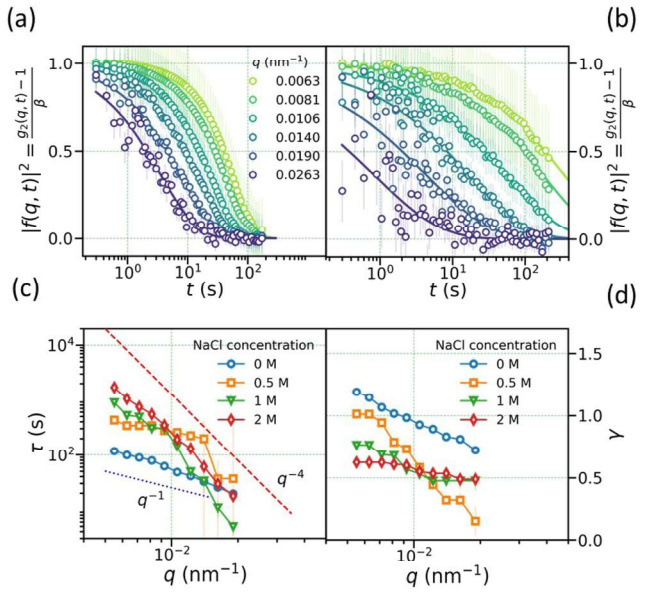

FIG. 4. Wave-vector dependent $|f(q,t)|^2$ of (a) yolk and (b) y2000 (yolk + 2M NaCl) at room temperature. The solid lines are fits using Eq. (2). The extracted fit parameters (c) τ and (d) γ at different salt concentrations. The dotted and dashed curves in (c) represent q^{-1} and q^{-4}, respectively.

with the addition of NaCl. To quantify the changes in the dynamics, ISFs are fitted using Eq. (2), and extracted relaxation times and KWW exponents are given in Figs. 4(c) and 4(d), respectively. Egg yolk shows ballistic-type dynamics ($\tau \propto q^{-1}$), which progressively changes to $\tau \propto q^{-4}$ dependence with increasing salt concentration. Such a peculiar q-dependence of the relaxation times has been predicted for the correlation functions of vibrating flexible fractal networks. Reuveni *et al.*[94] calculate that the correlation functions for such dynamics behave as $f(q,t) = \exp[-(t/\tau(q))^{\gamma}]$ with decorrelation times of the form $\tau \propto q^{-(2/\gamma)}$. Thus, our observations of $\tau(q) \propto q^{-4}$ and $\gamma = 0.5$ of the y2000 sample are in good agreement with this model for the dynamics of a flexible fractal network at $q\,Rg > 1$, where Rg is the gyration radius. The corresponding dynamics can be understood as being strongly influenced by the anomalous diffusion of the spatially averaged mean square displacement of a network bead.[94] Such a more fractal/fuzzy nature of the egg yolk granules upon salt addition is also in agreement with the observed changes in the $I(q)$ at T = 22 °C (Fig. 2).

B. Kinetics of thermal gelation of yolk at different NaCl concentrations

Figure 5(a) displays representative $I(q)$ curves during the gelation of the pure egg yolk sample at a temperature of T = 72 °C. Clearly, there is an increase in the scattering intensity for $q > 0.02$ nm^{-1}, reflecting the denaturation of yolk-plasma proteins.[52] The yolk-plasma proteins, such as γ– livetins, are the most unstable species in the yolk against temperature-induced changes and denature at temperatures as low as 60 °C.[95] Hence, the initial slow increase in scattering intensity is indicative of heat-induced protein denaturation. However, the intensity in the lower q-regime ($q < 0.02$ nm^{-1}) seems to be constant, suggesting the thermal stability of yolk-granules at T = 72 °C. Contrary to this observation, an overall increase in $I(q)$ is observed in the presence of NaCl [Fig. 5(b)], indicating the denaturation of yolk proteins. To quantify the rate of structural changes, we calculate the scattering invariant[52,53,56] using

$$Q = \int_{q_1}^{q_2} q^2 I(q)\, \mathrm{d}q. \tag{3}$$

The lower and upper limits of integration are q_1 = 0.02 nm^{-1} and q_2 = 0.17 nm^{-1}, respectively. Note that in pure yolk samples, an increase in intensity is observed in a q range of 0.02–0.2 nm^{-1} [Fig. 5(a)] and this is the rationale for choosing this q range for estimating Q. The estimated values of Q normalized with respect to the initial value $Q(t'_w = 0)$ for all samples are shown in Figs. 5(c)–5(f). We find the following similarities comparing the curves of all samples [Figs. 5(c)–5(f)]: (i) Q increases at all temperatures, (ii) the increase in Q during the heating time $t_{heating}$ (time to reach the set temperature from room temperature) is independent of the set temperature, and (iii) after reaching the set temperature, the rate at which Q grows depends on the temperature. In all cases, the growth kinetics get faster with increasing temperature, as expected.

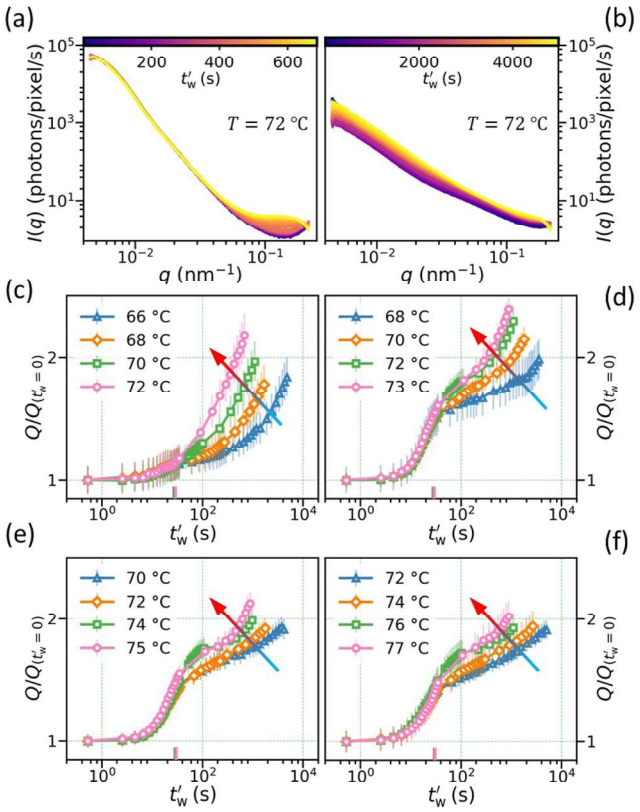

FIG. 5. Evolution of $I(q)$ of (a) pure egg yolk and (b) y2000 at $T = 72\,^{\circ}\mathrm{C}$. The color bar indicates the absolute waiting time t'_w from the onset of heating at 22 °C. The normalized scattering invariant $Q/Q_{(t'_w=0)}$ as a function of t'_w for (c) yolk, (d) y500, (e) y1000, and (f) y2000. The small vertical lines close to the horizontal-axis indicate $t_{heating}$ (time taken to reach the set temperature of 22 °C). The color of these lines matches that of data points at the same temperature. The arrows point in the direction of increasing temperatures.

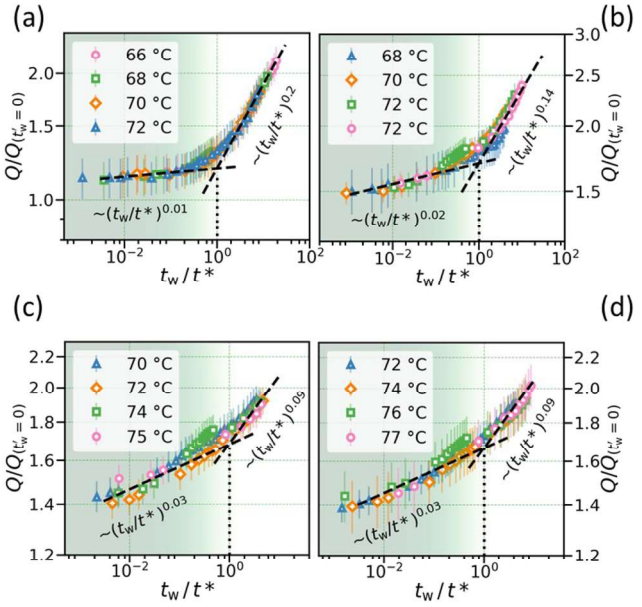

FIG. 6. Normalized scattering invariant $Q/Q_{(t'_w=0)}$ as a function of normalized isothermal waiting time t_w/t^* for (a) yolk, (b) y500, (c) y1000, and (d) y2000. The dashed lines indicate the power-law fits, and the power-law exponents are provided close to the dashed lines.

However, there are a few noticeable changes between pure and salted yolk samples. While there is a shallow increase in Q during the heating time ($t_{heating} \approx 26$–30 s) for the pure yolk sample [Fig. 5(c)], there is an exponential increase in Q for all salted yolk samples. Note that in salted samples, the yolk-granules are broken down and, hence, less robust. The exponential increase in the scattering intensity during the heating cycle could be an indication of the aggregate formation of these reactive species.

Furthermore, for a given temperature, the slope of Q increases with t'_w after $t_{heating}$ [Figs. 5(c)–5(f)]. To quantify these changes, we model the curves using a power-law function $Q/Q(t'_w = 0) \sim t_w^{\alpha}$ at low and high t_w. Note that isothermal waiting time $t_w = t'_w - t_{heating}$. For a given sample case, two power-law behaviors are observed at all temperatures, and the corresponding α values are independent of temperature. This implies a structural transition, and the transition time, t^*, is identified by the intersection of two power-law regimes. Here, t^* indicates the sol–gel transition time as reported in our earlier work.[52] The transition time t^* at each temperature T is an indicator of the isothermal heating time needed by the sample to form a gel from the liquid state.

The initial slow increase in Q points toward the denaturation of yolk proteins.[52] During this time, yolk proteins unfold their native structure, and the buried hydrophobic regions get exposed. This implies that stable proteins become more reactive, and the covalent and non-covalent interactions of these unfolded proteins lead to the formation of aggregates. The quick structural changes observed after t^* indicate the organization of protein aggregates, which leads to the formation of a three-dimensional (3D) gel network.

Interestingly, master curves are obtained after normalizing the time axis by t^* values, as depicted in Fig. 6. This implies the time-temperature superposition (TTS) of structural changes during yolk gelation, suggesting the same mechanism underlying the structural changes in each sample case with a temperature-dependent reaction rate. However, the power-law exponents (α) before and after t^* increase and decrease, respectively, with increasing salt concentration (Fig. 6). This indicates that the rate of evolution of structure during the heat-induced gelation is indeed affected by the addition of salt. The relevance of t^* becomes more evident when we compare the dynamical information with the underlying kinetic development in Sec. III. D.

C. Kinetics of LDL aggregation at different NaCl concentrations

In this section, we discuss the effect of the NaCl concentration on the aggregation of LDL molecules in egg yolk. When egg yolk is heated to $T > 75\,^{\circ}\mathrm{C}$, yolk-LDLs fuse, form aggregate, and give a

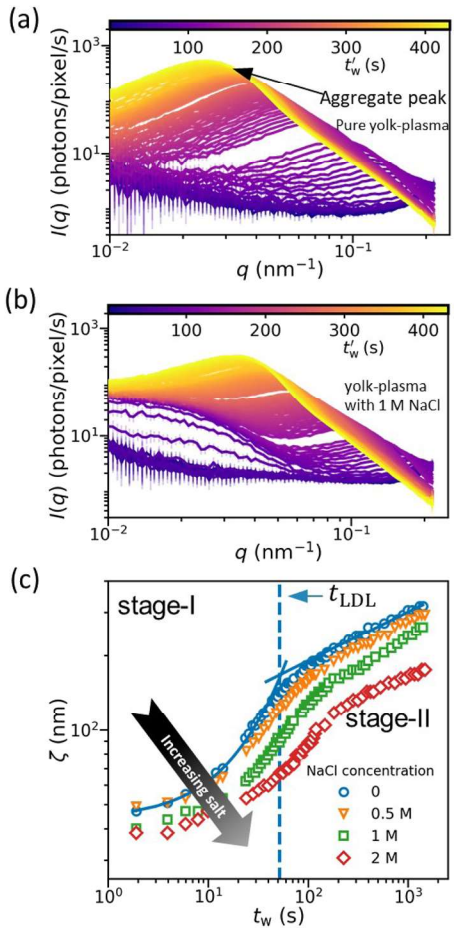

FIG. 7. Representative $I(q)$ profiles of yolk-plasma (a) without and (b) with 1M NaCl, collected at a sample temperature of $T = 90\,^{\circ}\mathrm{C}$ as a function of waiting time, t'_w as indicated by the color bar. (c) The correlation length ($\zeta = \frac{2\pi}{q_{peak}}$) estimated from the scattering profiles as a function of isothermal waiting time t_w for sample temperatures at different NaCl concentrations, as indicated in the legend. The exponential and power-law fits using Eqs. (5) and (6) on a pure yolk-plasma sample are depicted using solid curves. The intersection of these fits (t_{LDL}) is indicated by a dashed vertical line.

grainy microstructure to yolk gel.[52] Representative $I(q)$ curves of yolk-plasma heated to 90 °C are shown in Fig. 7(a). Aggregation of LDLs is indicated by the appearance of a peak at a higher q value (q_{peak}) and its movement to lower q values as t'_w increases. On comparing Figs. 7(a) and 7(b), a delay in the aggregation kinetics is observed with an increase in ionic strength. To analyze the kinetics of LDL aggregation, we extract the temporal evolution of the correlation length using,

$$\zeta = 2\pi/q_{peak}. \tag{4}$$

The estimated ζ values are shown in Fig. 7(c). Clearly, a delay in LDL aggregation kinetics is observed with an increase in the NaCl concentration.

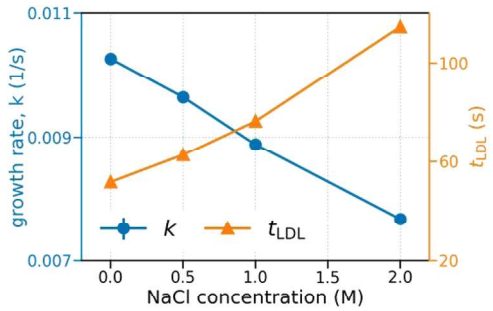

FIG. 8. Growth rate k and the crossover time, t_{LDL}, as a function of NaCl concentration.

A careful evaluation of individual ζ curves reveals two aggregation regimes.[52] An exponential growth phase (stage-I) is followed by a power-law growth phase (stage-II), as depicted in Fig. 7(c). The exponential growth reflects reaction-limited aggregation (RLA) kinetics, whereas power-law growth indicates diffusion-limited aggregation (DLA). In DLA, the rate of diffusion controls the aggregation process,[96] whereas in RLA, the rate of reaction controls the aggregation, meaning that a fraction of particle collisions lead to the formation of an aggregate.[97]

To quantify further, we model stage-I using,[98]

$$\zeta \propto e^{(kt_w)}, \tag{5}$$

where k gives the growth rate. Stage-II is modeled with a power-law function,[98]

$$\zeta \propto t_w^{\mu}, \tag{6}$$

where μ is the power-law exponent. The exponential and power-law fits using Eqs.(5) and (6), respectively, on ζ of a pure yolk sample are shown in Fig. 7(c). Interestingly, the growth rate, k, decreases with increasing salt concentration, as shown in Fig. 8. However, the power-law exponent is found to be unchanged ($\mu \approx 0.24 \pm 0.4$) with increasing salt concentration. The intersection of exponential (stage-I) and power-law (stage-II) fits gives the transition time, t_{LDL}, as depicted in Fig. 7(c). The t_{LDL} increases with increasing salt concentration (Fig. 8), reflecting the delay in LDL aggregation kinetics.

D. Microscopic dynamics of egg yolk gelation at different NaCl concentrations

In this section, we explore the effect of the NaCl concentration on the microscopic dynamics of egg yolk during thermal gelation. For this, we calculate the TTCs using Eq. (1). This results in a two-dimensional correlation map of intensity correlations at the experimental times t_1 and t_2, as shown in Figs. 9(a)–9(d). Every TTC in a single plot is collected from a new spot on the capillary, and the dynamics in each TTC are well connected to the neighboring TTCs. This seamless continuation suggests that the x-ray beam did not affect the sample dynamics during these measurements. In Fig. 9(a), the TTC of pure yolk heated to 72 °C is depicted. The

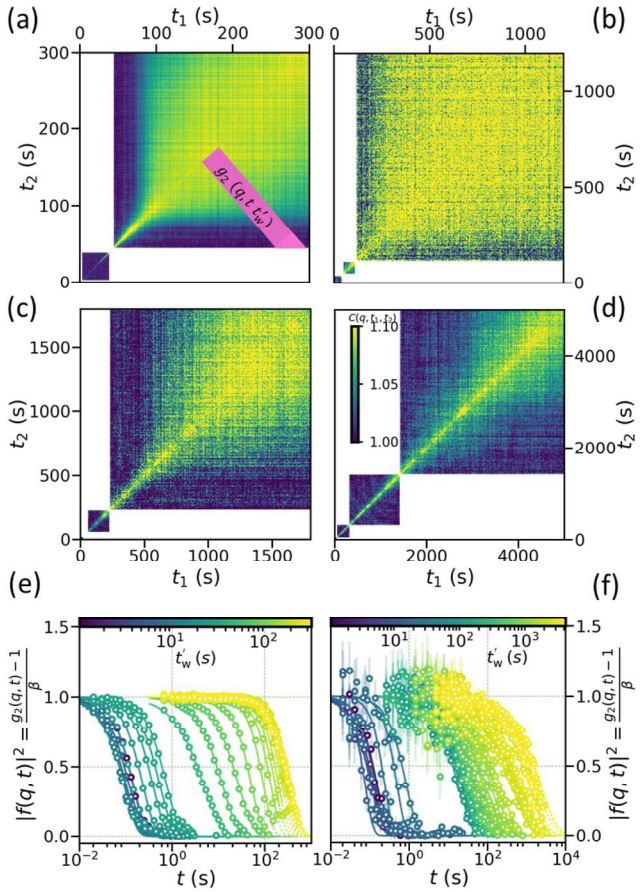

FIG. 9. Representative TTCs of (a) yolk, (b) y500, (c) y1000, and (d) y2000 during thermal gelation at $T = 72\,^{\circ}\mathrm{C}$ and $q = 0.0055\ \mathrm{nm}^{-1}$. The intermediate scattering functions of (e) yolk and (f) y2000 heated to 72 °C at different waiting times, as denoted by the color bar.

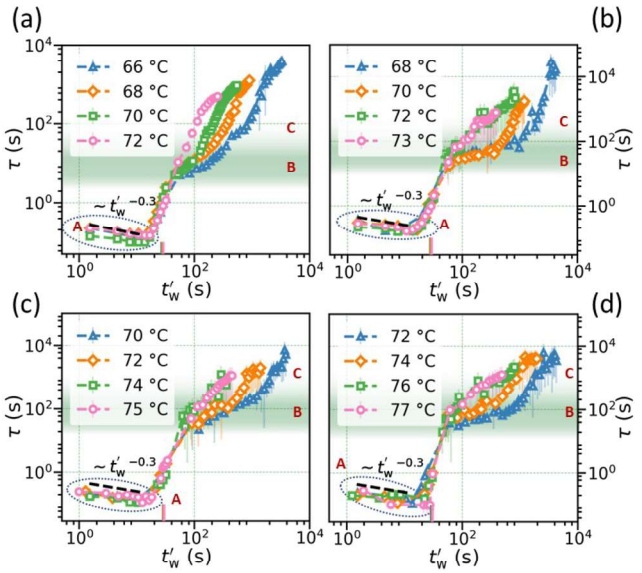

FIG. 10. Relaxation time of (a) yolk, (b) y500, (c) y1000, and (d) y2000 at several temperatures as mentioned in the legends. All τ values are extracted at $q = 0.0055\ \mathrm{nm}^{-1}$. The small vertical lines close to the horizontal-axis indicate t_{heating} (time taken to reach the set temperature of 22 °C). The color of these lines matches that of data points at the same temperature. The dynamic regime-A is represented by a dotted circle. Regime-B is represented by a green-colored region.

width of the yellow diagonal region of the TTC is directly proportional to the relaxation time of the system and the exponential increase in the width of the diagonal region at $t'_w \approx 80$ s, indicating the gelation of egg yolk at 72 °C. On comparing other TTCs at different salt concentrations [Figs. 9(a)–9(d)], it is evident that the gelation of egg yolk is considerably delayed by the addition of salt. To quantify these features, we extract the one-time correlation functions (g_2) from the TTCs. For this, we section a TTC into several diagonal slices. One such diagonal slice is depicted in Fig. 9(a). In the TTC, the diagonal axis represents sample age (t'_w), and the perpendicular lines to this axis are the one-time correlation functions as a function of the elapsed time $t = |t_1 - t_2|$. These cuts are called "constant sample age" cuts, which are used for further analysis.[77,81]

The intermediate scattering functions extracted from TTCs at different t'_w of yolk and y2000 are shown in Figs. 9(e) and 9(f), respectively, and the solid lines indicate the fits using Eq. (2). Interestingly, our data revealed a slow-down in the dynamics spanning five orders of magnitude (a fraction of a second to a few hours). The relaxation times extracted from the fit at $q = 0.0055\ \mathrm{nm}^{-1}$ for all samples are plotted in Fig. 10. As reported in our earlier work,[52] the temporal evolution of τ displays four distinct regimes (A, B, C, and D). In the present work, we have limited our experimental time scales to regime-C. The dynamical regime-A and regime-B are denoted by a dotted circle and a green-colored region in Fig. 10. When egg yolk is heated to room temperature, fast dynamics are observed in regime-A, indicating the fast motion of yolk-granules caused by thermal fluctuations. The steady decrease in τ $(\sim (t'_w)^{-0.3})$ in regime-A is attributed to the movement of the granules caused by an increase in their kinetic energy. After reaching the set temperature (indicated by the lines close to the horizontal-axis in Fig. 10), the system equilibrates at the final temperature, which is reflected by the sudden jump from regime-A to regime-B.

In regime-B, a shallow power-law slowdown in dynamics is observed, which indicates the denaturation of yolk proteins.[52] During regime-B, the egg yolk proteins unfold their native structure, exposing the hidden hydrophobic/sulfhydryl groups and forming aggregates through covalent and non-covalent interactions. Following this power-law behavior, there is an exponential slow-down in the dynamics observed in regime-C, indicating the solution-to-gel transition.

Normalized relaxation time with respect to the equilibrium relaxation time from regime-B as a function of normalized isothermal waiting time with respect to t^* (extracted from the kinetic evolution of the scattering intensity) gives a master curve as depicted

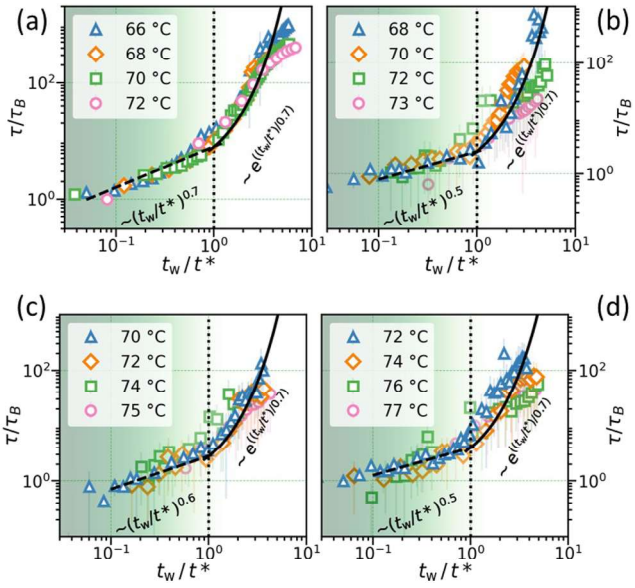

FIG. 11. Relaxation time normalized with respect to equilibrium relaxation time when the set temperature is reached (τ_B) for (a) yolk, (b) y500, (c) y1000, and (d) y2000 as a function of t_w normalized with respect to sol–gel transition time t^* (extracted from the kinetic evolution of the scattering intensity). The τ values are extracted at $q = 0.0055$ nm^{-1}. The dashed curve in the green-shaded region indicates the power-law fit, and the solid curve in the white region indicates the exponential fit.

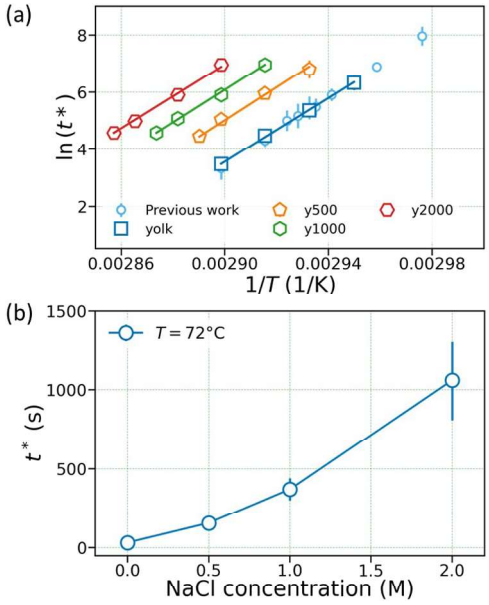

FIG. 12. (a) Arrhenius plot showing the temperature dependence of t^* at different NaCl concentrations. The circular data points are from our previous work.[52] The solid lines represent fits using Eq. (8). The extracted activation energy from the fits is 460 ± 20 kJ/mol. (b) t^* as a function of NaCl concentration at $T = 72$ °C.

in Fig. 11. This normalization helps to eliminate the variations in the τ of egg yolk samples due to the inherent heterogeneity of the sample volume. The shaded region on the left side of the plot represents regime-B. Clearly, the master curves obtained from kinetics (Fig. 6) and dynamics (Fig. 11) deliver complementary information on the evolution of the structure and dynamics of egg yolk during thermal gelation at different salt concentrations. This highlights the requirements of both structural and dynamic information while characterizing a non-equilibrium phenomenon such as gelation.

In addition, information about the nature of the dynamics can be obtained by following the evolution of the KWW exponent and the wave-vector dependence of τ ($\tau \propto q^{-p}$, where p is the exponent). The evolution of γ for all samples is provided in Figs. S7 and S8 of the supplementary material. We observe $\gamma \approx 1.5$ during the heating cycle and regime-B. γ then decreases in regime-C, reaching a minimum before slowly increasing again and reaching a value of 2 in the arrested gel phase.[78,84] Furthermore, the exponent p also varies while approaching t^*, as shown in Fig. S9 of the supplementary material. Close to the gel point, p increases, and the maximum of p is approximately close to the minimum of γ. Such behaviors are found close to phase transitions.[99,100] Further details can be found in the supplementary material.

In general, the activation energy barrier of the solution to gel transition can be extracted by modeling either the rate constant[101] or the characteristic time scales[102–106] using the Arrhenius equation. For this, we plot t^* in an Arrhenius plot, as shown in Fig. 12(a). As expected, the t^* values of yolk are in good agreement with our previous report.[52] To quantify this further, we model t^* values using the Arrhenius equation,[102,104]

$$t^* = Ae^{\left(\frac{E_a}{RT}\right)}, \tag{7}$$

$$\ln\,(t^*) = \frac{E_a}{RT} + \ln\,(A), \tag{8}$$

where E_a is the activation energy, R is the universal gas constant, and T is the temperature in Kelvin. The constant $1/A$ is known as the frequency factor or attempt frequency, as it gives the measure of the frequency of collisions.

The addition of NaCl does not significantly alter the activation energy of egg yolk gelation, which agrees with the results from differential scanning calorimetry.[107] The extracted activation energy from the fits is 460 ± 20 kJ/mol (≈110 kcal/mol, or 4.8 eV).

Interestingly, the sol–gel transition time at a specific temperature increases exponentially with NaCl concentration, as shown in Fig. 12(b). This implies that the gelation of egg yolk is significantly delayed with an increase in ionic strength. In other words, the rate of denaturation–aggregation–gelation is significantly affected by the ionic strength but not the gelation process itself, as the evolution of τ follows a master curve after normalization of time with sol–gel transition time (Fig. 11).

Next, we compare our results with those of other protein systems. Earlier studies[54] on the influence of NaCl on the heat-induced gelation of egg white reported an increase in the activation energy of gelation at higher salt concentrations. However, a decrease in activation energy with NaCl concentration was reported in whey protein fractal aggregates.[108] Nevertheless, no change in activation energy

was reported in the salt-induced gelation of soy-aggregates[19] with different concentrations of NaCl. Furthermore, the E_a of calcium- or acid-induced gelation of whey protein aggregates was not affected by the concentration of $CaCl_2$[109] or acid (HCl),[110] respectively, in the limited range investigated. This implies that different proteins behave differently with an increase in ionic strength, and this could be related to the charge density and structure of proteins.

The delay in the gelation of the yolk with NaCl could be attributed to the stability of the yolk constituents against temperature-induced denaturation. Miles *et al.*[111] describe two reasons that lead to the thermal stability of collagen fiber, which, although different in nature, can be employed for comparison and inspiration. The mechanisms are (i) the loss of chain entropy, which is brought about by the reduced number of molecular configurations available due to molecules being increasingly attached covalently in the presence of a cross-linking molecule, and (ii) the dehydration caused by subjecting the fiber to a low water activity environment. Some of these results could be extended to proteins as well. The addition of NaCl leads to the dehydration of proteins.[112] It is shown that dehydration stabilizes the folded structure of the proteins.[113] Hence, dehydration caused by the presence of NaCl provides more stability to proteins, and hence, the heat-induced denaturation rate is significantly reduced.

IV. CONCLUSION

In summary, we investigated (i) the changes to the structure and dynamics of egg yolk components upon the addition of NaCl (0.3–2 M) at room temperature and (ii) the influence of NaCl on the aggregation of yolk-LDLs and gelation of yolk-proteins at temperatures in the range of 66–90 °C by employing USAXS–XPCS. While yolk proteins and granules showed progressive changes in their structure with an increase in ionic strength, LDLs were found to restore their shape even at a 2M NaCl concentration. The rate of change of structural parameters during denaturation, aggregation, and gelation is found to be influenced by the change in ionic strength. However, the TTS relationship observed in all samples indicates an identical mechanism underlying protein aggregation–gelation with a temperature-dependent reaction rate. The sol–gel transition time extracted from structural and dynamical parameters follows Arrhenius behavior, and the activation energy of the gelation remained constant as the ionic strength increased.

SUPPLEMENTARY MATERIAL

See the supplementary material for the calibration of the Linkam heating cell and discussion of the x-ray beam influence on the structure and dynamics of egg yolk.

ACKNOWLEDGMENTS

We acknowledge DESY (Hamburg, Germany), a member of the Helmholtz Association HGF, for the provision of experimental facilities. Parts of this research were carried out at the beamline P10 during the allocated beamtime for Proposal No. II-20210008 and in-house beamtimes. The authors also thank the support of DFG (Grant No. NFDI 40/1), BMBF (Grant Nos. 05K19PS1, 05K20PSa, 05K22PS1, and 05K20VTA), and NFDI for this work. N.B. acknowledges the Alexander von Humboldt Foundation. M.P. thanks the DELTA machine group for providing synchrotron radiation for sample characterization.

AUTHOR DECLARATIONS

Conflict of Interest

The authors have no conflicts to disclose.

Author Contributions

Nimmi Das Anthuparambil: Conceptualization (lead); Data curation (lead); Formal analysis (lead); Investigation (lead); Methodology (lead); Visualization (lead); Writing – original draft (lead); Writing – review & editing (lead). **Sonja Timmermann**: Data curation (supporting); Investigation (supporting); Software (supporting); Writing – review & editing (supporting). **Michelle Dargasz**: Data curation (supporting); Investigation (supporting). **Sebastian Retzbach**: Data curation (supporting); Investigation (supporting); Writing – review & editing (supporting). **Maximilian D. Senft**: Data curation (supporting); Investigation (supporting). **Nafisa Begam**: Investigation (supporting); Writing – review & editing (supporting). **Anastasia Ragulskaya**: Investigation (supporting); Writing – review & editing (supporting). **Michael Paulus**: Data curation (supporting); Investigation (supporting); Writing – review & editing (supporting). **Fajun Zhang**: Validation (supporting); Writing – review & editing (supporting). **Fabian Westermeier**: Resources (equal); Supervision (supporting). **Michael Sprung**: Resources (equal); Software (equal); Supervision (supporting). **Frank Schreiber**: Funding acquisition (lead); Supervision (supporting); Validation (equal); Writing – review & editing (supporting). **Christian Gutt**: Funding acquisition (lead); Supervision (equal); Validation (equal); Visualization (equal); Writing – original draft (equal); Writing – review & editing (equal).

DATA AVAILABILITY

Raw data were generated at PETRA III, Hamburg, Germany. Derived data supporting the findings of this study are available from the corresponding author upon reasonable request.

REFERENCES

[1] J. F. Zayas, "Gelling properties of proteins," in *Functionality of Proteins in Food* (Springer, Berlin, Heidelberg, 1997), pp. 310–366.
[2] R. Huopalahti, M. Anton, R. López-Fandiño, and R. Schade, *Bioactive Egg Compounds* (Springer, Berlin, 2007), Vol. 5.
[3] T. Nicolai, "Gelation of food protein-protein mixtures," Adv. Colloid Interface Sci. **270**, 147–164 (2019).
[4] K. B. Djagny, Z. Wang, and S. Xu, "Gelatin: A valuable protein for food and pharmaceutical industries: Review," Crit. Rev. Food Sci. Nutr. **41**, 481–492 (2001).
[5] M. L. Floren, S. Spilimbergo, A. Motta, and C. Migliaresi, "Carbon dioxide induced silk protein gelation for biomedical applications," Biomacromolecules **13**, 2060–2072 (2012).
[6] A. Rodil *et al.*, "Gels prepared from egg yolk and its fractions for tissue engineering," Biotechnol. Prog. **32**, 1577–1583 (2016).

[7]Y. Mine, *Egg Bioscience and Biotechnology* (John Wiley & Sons, 2008).
[8]P.-O. Hegg, H. Martens, and B. Löfqvist, "Effects of pH and neutral salts on the formation and quality of thermal aggregates of ovalbumin. a study on thermal aggregation and denaturation," J. Sci. Food Agric. **30**, 981–993 (1979).
[9]Y. Ma and F. Chen, "Plant protein heat-induced gels: Formation mechanisms and regulatory strategies," Coatings **13**, 1899 (2023).
[10]F. Van Kleef, "Thermally induced protein gelation: Gelation and rheological characterization of highly concentrated ovalbumin and soybean protein gels," Biopolymers **25**, 31–59 (1986).
[11]Z. Ju and A. Kilara, "Textural properties of cold-set gels induced from heat-denatured whey protein isolates," J. Food Sci. **63**, 288–292 (1998).
[12]C. Au, N. C. Acevedo, H. T. Horner, and T. Wang, "Determination of the gelation mechanism of freeze–thawed hen egg yolk," J. Agric. Food Chem. **63**, 10170–10180 (2015).
[13]X. Ma, R. Feng, L. Ahrné, and V. Orlien, "Pressure-induced gelation of blended milk and pea protein suspensions," Food Hydrocolloids **146**, 109284 (2024).
[14]A. Totosaus, J. G. Montejano, J. A. Salazar, and I. Guerrero, "A review of physical and chemical protein-gel induction," Int. J. Food Sci. Technol. **37**, 589–601 (2002).
[15]N. Chen, M. Zhao, C. Chassenieux, and T. Nicolai, "The effect of adding NaCl on thermal aggregation and gelation of soy protein isolate," Food Hydrocolloids **70**, 88–95 (2017).
[16]Y. Zhao, F. Feng, Y. Yang, C. Xiong, M. Xu, and Y. Tu, "Gelation behavior of egg yolk under physical and chemical induction: A review," Food Chem. **355**, 129569 (2021).
[17]Z. Yang, L. de Campo, E. P. Gilbert, R. Knott, L. Cheng, B. Storer, X. Lin, L. Luo, S. Patole, and Y. Hemar, "Effect of NaCl and $CaCl_2$ concentration on the rheological and structural characteristics of thermally-induced quinoa protein gels," Food Hydrocolloids **124**, 107350 (2022).
[18]K. Ako, T. Nicolai, and D. Durand, "Salt-induced gelation of globular protein aggregates: Structure and kinetics," Biomacromolecules **11**, 864–871 (2010).
[19]N. Chen, C. Chassenieux, and T. Nicolai, "Kinetics of NaCl induced gelation of soy protein aggregates: Effects of temperature, aggregate size, and protein concentration," Food Hydrocolloids **77**, 66–74 (2018).
[20]C. Tanger, M. Müller, D. Andlinger, and U. Kulozik, "Influence of pH and ionic strength on the thermal gelation behaviour of pea protein," Food Hydrocolloids **123**, 106903 (2022).
[21]D. Perez, F. Harte, and T. Lopez-Pedemonte, "Ionic strength and buffering capacity of emulsifying salts determine denaturation and gelation temperatures of whey proteins," J. Dairy Sci. **105**, 7230–7241 (2022).
[22]M. Sadeghi, A. Madadlou, A. Khosrowshahi, and M. Mohammadifar, "Acid-induced gelation behavior of casein/whey protein solutions assessed by oscillatory rheology," J. Food Sci. Technol. **51**, 2113–2119 (2014).
[23]Y. Lian, Y. Li, R. Lv, L. Wang, and W. Xiong, "The mechanism of alkali-induced rice protein gel formation: Effect of alkali concentration and temperature," Food Hydrocolloids **147**, 109335 (2024).
[24]X. Gao, Y. Yao, N. Wu, M. Xu, Y. Zhao, and Y. Tu, "The sol-gel-sol transformation behavior of egg white proteins induced by alkali," Int. J. Biol. Macromol. **155**, 588–597 (2020).
[25]N. Yuno-Ohta, T. Higasa, E. Tatsumi, H. Sakurai, R. Asano, and M. Hirose, "Formation of fatty acid salt-induced gel of ovalbumin and the mechanism for gelation," J. Agric. Food Chem. **46**, 4518–4523 (1998).
[26]N. Nio, M. Motoki, and K. Takinami, "Gelation mechanism of protein solution by transglutaminase," Agric. Biol. Chem. **50**, 851–855 (1986).
[27]J. M. Renkema, H. Gruppen, and T. Van Vliet, "Influence of pH and ionic strength on heat-induced formation and rheological properties of soy protein gels in relation to denaturation and their protein compositions," J. Agric. Food Chem. **50**, 6064–6071 (2002).
[28]Z.-W. Wu, X.-L. Zou, P.-L. Yao, Z.-L. Kang, and H.-J. Ma, "Changes in gel characteristics, rheological properties, and water migration of pse meat myofibrillar proteins with different amounts of sodium bicarbonate," Molecules **27**, 8853 (2022).
[29]S. D. Arntfield, E. D. Murray, and M. A. H. Ismond, "Influence of salts on the microstructural and rheological properties of heat-induced protein networks from ovalbumin and vicilin," J. Agric. Food Chem. **38**, 1335–1343 (1990).
[30]Y.-I. Kinekawa, T. Fuyuki, and N. Kitabatake, "Effects of salts on the properties of sols and gels prepared from whey protein isolate and process whey protein," J. Dairy Sci. **81**, 1532–1544 (1998).
[31]Y. Lei, H. Ouyang, W. Peng, X. Yu, L. Jin, and S. Li, "Effect of NaCl on the rheological, structural, and gelling properties of walnut protein isolate-κ-carrageenan composite gels," Gels **8**, 259 (2022).
[32]Y. Zhang, G. Bai, G. Jin, Y. Wang, J. Wang, E. Puolanne, and J. Cao, "Role of low molecular additives in the myofibrillar protein gelation: Underlying mechanisms and recent applications," Crit. Rev. Food Sci. Nutr. **64**, 3604–3622 (2024).
[33]M. Primacella, T. Fei, N. Acevedo, and T. Wang, "Effect of food additives on egg yolk gelation induced by freezing," Food Chem. **263**, 142–150 (2018).
[34]J. Li, J. Zhai, L. Gu, Y. Su, L. Gong, Y. Yang, and C. Chang, "Hen egg yolk in food industry—A review of emerging functional modifications and applications," Trends Food Sci. Technol. **115**, 12–21 (2021).
[35]A. Laca, B. Paredes, M. Rendueles, and M. Díaz, "Egg yolk granules: Separation, characteristics and applications in food industry," LWT-Food Sci. Technol. **59**, 1–5 (2014).
[36]L. Gu, Y. Liu, W. Zhang, J. Li, C. Chang, Y. Su, and Y. Yang, "Novel extraction technologies and potential applications of egg yolk proteins," Food Sci. Biotechnol. **32**, 121–133 (2023).
[37]M. Anton, "Egg yolk: Structures, functionalities and processes," J. Sci. Food Agric. **93**, 2871–2880 (2013).
[38]S.-C. Yang and R. E. Baldwin, "Functional properties of eggs in foods," in *Egg Science and Technology* (CRC Press, 2017), pp. 405–463.
[39]T. Weiss, "Mayonnaise and salad dressings," in *Food Oils and Their Uses* (The AVI Publishing Company, 1970), pp. 145–176.
[40]B. Lowe, *Experimental Cookery from the Chemical and Physical Standpoint* (John Wiley Sons, Inc.; Chapman Hall, Limited, New York; London, 1955) Chap. Emulsions.
[41]M. Taslikh, N. Mollakhalili-Meybodi, A. M. Alizadeh, M.-M. Mousavi, K. Nayebzadeh, and A. M. Mortazavian, "Mayonnaise main ingredients influence on its structure as an emulsion," J. Food Sci. Technol. **59**, 2108–2116 (2022).
[42]L. Harrison and F. Cunningham, "Influence of salt on properties of liquid yolk and functionality in mayonnaise," Poult. Sci. **65**, 915–921 (1986).
[43]S.-S. Yang and O. J. Cotterill, "Physical and functional properties of 10% salted egg yolk in mayonnaise," J. Food Sci. **54**, 210–213 (1989).
[44]J. Aguilar, F. Cordobés, C. Bengoechea, and A. Guerrero, "Heat-induced gelation of egg yolk as a function of pH. does the type of acid make any difference?," Food Hydrocolloids **87**, 142–148 (2019).
[45]P. Hongsprabhas and S. Barbut, "Protein and salt effects on Ca^{2+}-induced cold gelation of whey protein isolate," J. Food Sci. **62**, 382–385 (1997).
[46]C. Bryant and D. McClements, "Influence of NaCl and $CaCl_2$ on cold-set gelation of heat-denatured whey protein," J. Food Sci. **65**, 801–804 (2000).
[47]X. D. Sun and S. D. Arntfield, "Dynamic oscillatory rheological measurement and thermal properties of pea protein extracted by salt method: Effect of pH and NaCl," J. Food Eng. **105**, 577–582 (2011).
[48]J.-L. Mession, N. Sok, A. Assifaoui, and R. Saurel, "Thermal denaturation of pea globulins (*Pisum sativum* L.)—Molecular interactions leading to heat-induced protein aggregation," J. Agric. Food Chem. **61**, 1196–1204 (2013).
[49]X. Lv, X. Huang, B. Ma, Y. Chen, Z. Batool, X. Fu, and Y. Jin, "Modification methods and applications of egg protein gel properties: A review," Compr. Rev. Food Sci. Food Saf. **21**, 2233–2252 (2022).
[50]J. Li, X. Li, C. Wang, M. Zhang, Y. Xu, B. Zhou, Y. Su, and Y. Yang, "Characteristics of gelling and water holding properties of hen egg white/yolk gel with nacl addition," Food Hydrocolloids **77**, 887–893 (2018).
[51]T. Kaewmanee, S. Benjakul, W. Visessanguan, and C. Gamonpilas, "Effect of sodium chloride and osmotic dehydration on viscoelastic properties and thermal-induced transitions of duck egg yolk," Food Bioprocess Technol. **6**, 367–376 (2013).
[52]N. D. Anthuparambil, A. Girelli, S. Timmermann, M. Kowalski, M. S. Akhundzadeh, S. Retzbach, M. D. Senft, M. Dargasz, D. Gutmüller, A. Hiremath *et al.*, "Exploring non-equilibrium processes and spatio-temporal scaling laws in heated egg yolk using coherent X-rays," Nat. Commun. **14**, 5580 (2023).
[53]N. Begam *et al.*, "Kinetics of network formation and heterogeneous dynamics of an egg white gel revealed by coherent X-ray scattering," Phys. Rev. Lett. **126**, 098001 (2021).

[54]N. Begam, S. Timmermann, A. Ragulskaya, A. Girelli, M. D. Senft, S. Retzbach, N. D. Anthuparambil, M. S. Akhundzadeh, M. Kowalski, M. Reiser *et al.*, "Effects of temperature and ionic strength on the microscopic structure and dynamics of egg white gels," J. Chem. Phys. **158**, 074903 (2023).
[55]S. Timmermann, N. D. Anthuparambil, A. Girelli, N. Begam, M. Kowalski, S. Retzbach, M. D. Senft, M. S. Akhundzadeh, H.-F. Poggemann, M. Moron *et al.*, "X-ray driven and intrinsic dynamics in protein gels," Sci. Rep. **13**, 11048 (2023).
[56]M. Moron *et al.*, "Gelation dynamics upon pressure-induced liquid–liquid phase separation in a water–lysozyme solution," J. Phys. Chem. B **126**, 4160–4167 (2022).
[57]A. Girelli *et al.*, "Microscopic dynamics of liquid-liquid phase separation and domain coarsening in a protein solution revealed by X-ray photon correlation spectroscopy," Phys. Rev. Lett. **126**, 138004 (2021).
[58]A. Ragulskaya, N. Begam, A. Girelli, H. Rahmann, M. Reiser, F. Westermeier, M. Sprung, F. Zhang, C. Gutt, and F. Schreiber, "Interplay between kinetics and dynamics of liquid–liquid phase separation in a protein solution revealed by coherent X-ray spectroscopy," J. Phys. Chem. Lett. **12**, 7085–7090 (2021).
[59]N. Das, N. Begam, M. Ibrahim, S. Chandran, V. Padmanabhan, M. Sprung, and J. Basu, "Viscosity and fragility of confined polymer nanocomposites: A tale of two interfaces," Nanoscale **11**, 8546–8553 (2019).
[60]N. Begam, N. Das A, S. Chandran, M. Ibrahim, V. Padmanabhan, M. Sprung, and J. K. Basu, "Nanoparticle–polymer interfacial layer properties tune fragility and dynamic heterogeneity of athermal polymer nanocomposite films," Soft Matter **14**, 8853–8859 (2018).
[61]N. Das A, N. Begam, S. Chandran, A. Swain, M. Sprung, and J. K. Basu, "Thermal stability and dynamics of soft nanoparticle membranes: Role of entropy, enthalpy and membrane compressibility," Soft Matter **16**, 1117–1124 (2020).
[62]A. Jain, F. Schulz, I. Lokteva, L. Frenzel, G. Grübel, and F. Lehmkühler, "Anisotropic and heterogeneous dynamics in an aging colloidal gel," Soft Matter **16**, 2864–2872 (2020).
[63]B. Ruta, G. Baldi, Y. Chushkin, B. Rufflé, L. Cristofolini, A. Fontana, M. Zanatta, and F. Nazzani, "Revealing the fast atomic motion of network glasses," Nat. Commun. **5**, 3939 (2014).
[64]Q. Zhang, E. M. Dufresne, and A. R. Sandy, "Dynamics in hard condensed matter probed by X-ray photon correlation spectroscopy: Present and beyond," Curr. Opin. Solid State Mater. Sci. **22**, 202–212 (2018).
[65]J. Song, Q. Zhang, F. de Quesada, M. H. Rizvi, J. B. Tracy, J. Ilavsky, S. Narayanan, E. Del Gado, R. L. Leheny, N. Holten-Andersen, and G. H. McKinley, "Microscopic dynamics underlying the stress relaxation of arrested soft materials," Proc. Natl. Acad. Sci. U. S. A. **119**, e2201566119 (2022).
[66]W. J. Stadelman and O. J. Cotterill, *Egg Science and Technology*, 4th ed. (CRC Press, Boca Raton, 1995).
[67]C. Chang, W. Powrie, and O. Fennema, "Microstructure of egg yolk," J. Food Sci. **42**, 1193–1200 (1977).
[68]R. Bellairs, "The structure of the yolk of the hen's egg as studied by electron microscopy: I. The yolk of the unincubated egg," J. Cell Biol. **11**, 207–225 (1961).
[69]L. Xu, Y. Zhao, M. Xu, Y. Yao, N. Wu, H. Du, and Y. Tu, "Changes in physicochemical properties, microstructure, protein structures and intermolecular force of egg yolk, plasma and granule gels during salting," Food Chem. **275**, 600–609 (2019).
[70]M. Anton, M. L. Denmat, and G. Gandemer, "Thermostability of hen egg yolk granules: Contribution of native structure of granules," J. Food Sci. **65**, 581–584 (2000).
[71]T. Strixner, J. Sterr, U. Kulozik, and R. Gebhardt, "Structural study on hen-egg yolk high density lipoprotein (HDL) granules," Food Biophys. **9**, 314–321 (2014).
[72]B. M. Oladimeji and R. Gebhardt, "Physical characteristics of egg yolk granules and effect on their functionality," Foods **12**, 2531 (2023).
[73]M. Reiser *et al.*, "Resolving molecular diffusion and aggregation of antibody proteins with megahertz X-ray free-electron laser pulses," Nat. Commun. **13**, 5528 (2022).
[74]G. Pintori, G. Baldi, B. Ruta, and G. Monaco, "Relaxation dynamics induced in glasses by absorption of hard x-ray photons," Phys. Rev. B **99**, 224206 (2019).
[75]Y. Chushkin *et al.*, "Probing cage relaxation in concentrated protein solutions by X-ray photon correlation spectroscopy," Phys. Rev. Lett. **129**, 238001 (2022).
[76]M. Reiser and R. Rosca (2019). "Xana," Github. https://github.com/reiserm/Xana
[77]O. Bikondoa, "On the use of two-time correlation functions for X-ray photon correlation spectroscopy data analysis," J. Appl. Crystallogr. **50**, 357–368 (2017).
[78]A. Madsen, R. L. Leheny, H. Guo, M. Sprung, and O. Czakkel, "Beyond simple exponential correlation functions and equilibrium dynamics in x-ray photon correlation spectroscopy," New J. Phys. **12**, 055001 (2010).
[79]O. G. Shpyrko, "X-ray photon correlation spectroscopy," J. Synchrotron Radiat. **21**, 1057–1064 (2014).
[80]A. Ragulskaya *et al.*, "Reverse-engineering method for XPCS studies of non-equilibrium dynamics," IUCrJ **9**, 439 (2022).
[81]A. Ragulskaya, V. Starostin, F. Zhang, C. Gutt, and F. Schreiber, "On the analysis of two-time correlation functions: Equilibrium vs non-equilibrium systems," J. Appl. Crystallogr. **57**, 4 (2024).
[82]F. Perakis and C. Gutt, "Towards molecular movies with X-ray photon correlation spectroscopy," Phys. Chem. Chem. Phys. **22**, 19443–19453 (2020).
[83]G. Williams and D. C. Watts, "Non-symmetrical dielectric relaxation behaviour arising from a simple empirical decay function," Trans. Faraday Soc. **66**, 80–85 (1970).
[84]L. Cipelletti, L. Ramos, S. Manley, E. Pitard, D. A. Weitz, E. E. Pashkovski, and M. Johansson, "Universal non-diffusive slow dynamics in aging soft matter," Faraday Discuss. **123**, 237–251 (2003).
[85]A. Fluerasu, A. Moussaïd, A. Madsen, and A. Schofield, "Slow dynamics and aging in colloidal gels studied by x-ray photon correlation spectroscopy," Phys. Rev. E **76**, 010401 (2007).
[86]B. Chung, S. Ramakrishnan, R. Bandyopadhyay, D. Liang, C. Zukoski, J. Harden, and R. Leheny, "Microscopic dynamics of recovery in sheared depletion gels," Phys. Rev. Lett. **96**, 228301 (2006).
[87]B. Ruta, G. Baldi, G. Monaco, and Y. Chushkin, "Compressed correlation functions and fast aging dynamics in metallic glasses," J. Chem. Phys. **138**, 054508 (2013).
[88]E. M. Anitas, "Small-angle scattering from mass and surface fractals," in *Complexity in Biological and Physical Systems*, edited by R. López-Ruiz (IntechOpen, Rijeka, 2017), Chap. 10.
[89]P. W. Schmidt, "A review of some recent applications of small-angle scattering in studies of polydisperse systems and porous materials," in *Makromolekulare Chemie. Macromolecular Symposia* (Wiley Online Library, 1988), Vol. 15, pp. 153–166.
[90]C. Sorensen, "Light scattering by fractal aggregates: A review," Aerosol Sci. Technol. **35**, 648–687 (2001).
[91]T. Li, H. Su, J. Zhu, and Y. Fu, "Janus effects of nacl on structure of egg yolk granules," Food Chem. **371**, 131077 (2022).
[92]Y. Fu, J. Yao, H. Su, and T. Li, "Effects of calcium chelators on colloidal stability and interfacial activity of egg yolk granules," Food Biophys. **17**, 302–313 (2022).
[93]D. Causeret, E. Matringe, and D. Lorient, "Ionic strength and pH effects on composition and microstructure of yolk granules," J. Food Sci. **56**, 1532–1536 (1991).
[94]S. Reuveni, J. Klafter, and R. Granek, "Dynamic structure factor of vibrating fractals," Phys. Rev. Lett. **108**, 068101 (2012).
[95]D. Dixon and O. Cotterill, "Electrophoretic and chromatographic changes in egg yolk proteins due to heat," J. Food Sci. **46**, 981–983 (1981).
[96]M. Lin, H. Lindsay, D. Weitz, R. Klein, R. Ball, and P. Meakin, "Universal diffusion-limited colloid aggregation," J. Phys.: Condens. Matter **2**, 3093 (1990).
[97]R. C. Ball, D. A. Weitz, T. A. Witten, and F. Leyvraz, "Universal kinetics in reaction-limited aggregation," Phys. Rev. Lett. **58**, 274 (1987).
[98]F. Zhang, D. G. Dressen, M. W. Skoda, R. M. Jacobs, S. Zorn, R. A. Martin, C. M. Martin, G. F. Clark, and F. Schreiber, "Gold nanoparticles decorated with oligo (ethylene glycol) thiols: Kinetics of colloid aggregation driven by depletion forces," Eur. Biophys. J. **37**, 551–561 (2008).
[99]L. Frenzel, M. Dartsch, G. M. Balaguer, F. Westermeier, G. Grübel, and F. Lehmkühler, "Glass-liquid and glass-gel transitions of soft-shell particles," Phys. Rev. E **104**, L012602 (2021).

[100]V. Nigro, B. Ruzicka, B. Ruta, F. Zontone, M. Bertoldo, E. Buratti, and R. Angelini, "Relaxation dynamics, softness, and fragility of microgels with interpenetrated polymer networks," Macromolecules **53**, 1596–1603 (2020).
[101]R. Mercadé-Prieto, R. J. Falconer, W. R. Paterson, and D. I. Wilson, "Effect of gel structure on the dissolution of heat-induced β-lactoglobulin gels in alkali," J. Agric. Food Chem. **54**, 5437–5444 (2006).
[102]C. Vega and R. Mercadé-Prieto, "Culinary biophysics: On the nature of the 6X °C egg," Food Biophys. **6**, 152–159 (2011).
[103]C. Le Bon, T. Nicolai, and D. Durand, "Kinetics of aggregation and gelation of globular proteins after heat-induced denaturation," Macromolecules **32**, 6120–6127 (1999).
[104]M. Lu, D. L. Gantz, H. Herscovitz, and O. Gursky, "Kinetic analysis of thermal stability of human low density lipoproteins: A model for LDL fusion in atherogenesis," J. Lipid Res. **53**, 2175–2185 (2012).
[105]L. Huang, R. Takahashi, S. Kobayashi, T. Kawase, and K. Nishinari, "Gelation behavior of native and acetylated konjac glucomannan," Biomacromolecules **3**, 1296–1303 (2002).
[106]T. Phan-Xuan, D. Durand, T. Nicolai, L. Donato, C. Schmitt, and L. Bovetto, "On the crucial importance of the pH for the formation and self-stabilization of protein microgels and strands," Langmuir **27**, 15092–15101 (2011).
[107]N. Shibata-Ishiwatari, T. Takagi, M. Fukuoka, and N. Sakai, "Kinetic studies on the effect of salt on the thermal denaturation of egg constituents," Jpn. J. Food Eng. **19**, 49–56 (2018).
[108]A. Kharlamova, T. Nicolai, and C. Chassenieux, "Gelation of whey protein fractal aggregates induced by the interplay between added HCL, $CaCl_2$, and NaCl," Int. Dairy J. **111**, 104824 (2020).
[109]A. Kharlamova, T. Nicolai, and C. Chassenieux, "Calcium-induced gelation of whey protein aggregates: Kinetics, structure and rheological properties," Food Hydrocolloids **79**, 145–157 (2018).
[110]A. Kharlamova, C. Chassenieux, and T. Nicolai, "Acid-induced gelation of whey protein aggregates: Kinetics, gel structure and rheological properties," Food Hydrocolloids **81**, 263–272 (2018).
[111]C. A. Miles, N. C. Avery, V. V. Rodin, and A. J. Bailey, "The increase in denaturation temperature following cross-linking of collagen is caused by dehydration of the fibres," J. Mol. Biol. **346**, 551–556 (2005).
[112]O. S. Lawal, K. O. Adebowale, B. Ogunsanwo, O. Sosanwo, and S. Bankole, "On the functional properties of globulin and albumin protein fractions and flours of African locust bean (*parkia biglobossa*)," Food Chem. **92**, 681–691 (2005).
[113]M. Hishida, A. Kaneko, Y. Yamamura, and K. Saito, "Contrasting changes in strongly and weakly bound hydration water of a protein upon denaturation," J. Phys. Chem. C **127**, 6296–6305 (2023).